

# Analysis of Functional Connectivity and its Fusion with Multi-Omics Using Contrastive Learning

## Prospectus

Anton Orlichenko  
Advisor/Committee Chair: Yu-Ping Wang

Committee Members:  
Zhengming Ding, Hong-Wen Deng, Donald Gaver

Department of Biomedical Engineering  
Tulane University

June 2023

### Abstract

In the past, treatment was carried out with limited knowledge of patient endophenotype, derived only from blood work or vital signs taken at examination. Currently, greater appreciation is being given to the heterogeneity of patient groups and the differential effects of treatments and medications on those groups. This is evidenced by the National Institute of Mental Health's (NIMH's) Research Domain Criteria (RDoC), an attempt to perform psychiatric diagnosis and treatment based on quantitative neurological processes. The goal of this project is to utilize multi-modal imaging and genomics to integrate multiscale brain connectomes with genetic factors in order to untangle the neurological mechanisms of both normal development and disease progression.

This work focuses on the creation of models and tools to fuse functional brain imaging with multi-omics as well as on mitigating several of the problems of brain imaging. First, we will create models that work well in the low sample size, high dimensionality regime characteristic of most imaging studies. Second, we will create a tool for the rapid exploration and quality control of fMRI datasets, and show how it can be used to identify a previously unreported race confound. Third, we will explore the nature of functional connectivity by creating a data-efficient generative model. Besides achieving almost perfect subject identifiability and modest classification improvement, our model allows for the creation of synthetic

subjects based on clinical characteristics, aiding in understanding and interpretability. Finally, we will combine our earlier work with the well-studied paradigm of contrastive learning in order to both take advantage of large, unlabeled imaging datasets as well as to make associations between imaging and genomics.

## Contents

<b>1 Specific Aims</b>	<b>3</b>
1.1 Aim 1: Models for Small Sample Size, High Dimensionality Datasets	3
1.2 Aim 2: Tools for Data Exploration and Identification of Confounds	3
1.3 Aim 3: A Generative Model for Functional Connectivity . . . . .	4
1.4 Aim 4: Contrastive Learning for Fusing Omics with Brain Imaging	4
<b>2 Background &amp; Significance</b>	<b>5</b>
2.1 Cognitive Science and Mental Illness . . . . .	5
2.2 fMRI and Functional Connectivity . . . . .	5
2.3 Decompositions and Generative Models . . . . .	8
2.4 Contrastive Learning and Data Fusion . . . . .	10
<b>3 Research Project Description</b>	<b>12</b>
3.1 Aim 1: Latent Similarity Identifies Important Functional Connections for Phenotype Prediction . . . . .	12
3.2 Aim 2: ImageNomer: developing an fMRI and omics visualization tool to detect racial bias in functional connectivity . . . . .	16
3.3 Aim 3: Angle Basis: A Generative Model and Decomposition for Functional Connectivity . . . . .	18
3.4 Aim 4: Contrastive Learning for Fusing Omics with Brain Imaging	23
<b>4 Timeline</b>	<b>26</b>
4.1 Fall 2022: Aim 1 - Latent Similarity . . . . .	26
4.2 Spring 2023: Aim 2 - ImageNomer . . . . .	26
4.3 Fall 2023: Aim 3 - Angle Basis . . . . .	26
4.4 Spring 2024: Aim 4 - Contrastive Learning and Omics Fusion . .	26
4.5 Fall 2024: Dissertation . . . . .	26
<b>A Dynamic Dictionary Entries are Rank-1 Functional Connectivity Networks Associated with Maturation</b>	<b>36</b>

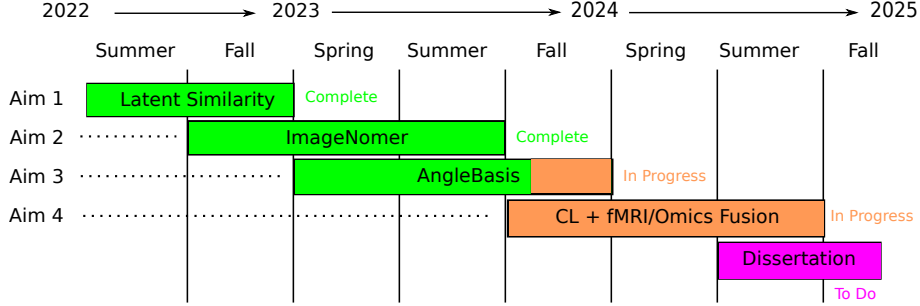


Figure 1: Aims and projected timeline for dissertation research.

## 1 Specific Aims

### 1.1 Aim 1: Models for Small Sample Size, High Dimensionality Datasets

We will create a model that is robust at the small sample sizes and high feature dimensionality found in typical fMRI studies. It should also give similar prediction performance compared to traditional ML models when trained on larger numbers of subjects. In addition, the model should be computationally efficient, and take a fraction of the computing time of deep models. To do this, we will leverage a kernel-based projection to a low-dimensional space, followed by calculation of pairwise similarities, finally followed by softmax aggregation. Additionally, the gradient-based computational framework will allow useful operations such as feature disentanglement and modality alignment. Important features will be selected by a bootstrapped greedy selection algorithm using Latent Similarity in its inner loop.

### 1.2 Aim 2: Tools for Data Exploration and Identification of Confounds

One of the major working problems with research is the curation and exploration of datasets, both large and small. This is important for quickly identifying basic trends in demographics as well as for performing quality control. To this end, we create ImageNomer, a web-based tool that finds correlations between fMRI features and demographics and is able to visualize the weights of machine learning models. We use ImageNomer to quickly identify a potential confounding effect of race on age-corrected achievement scores. Further analysis with the tool reveals that fMRI-achievement correlation is a subset of fMRI-race correlation. This is confirmed by comparing whole-cohort to within-ethnicity predictive models. We expect to use the tool in future studies.

### **1.3 Aim 3: A Generative Model for Functional Connectivity**

Functional connectivity (FC) is among the most widely used inputs for fMRI-based predictive models, owing to its simplicity and robustness. However, theoretical models for the analysis of FC are lacking. Using a basis of sine waves combined with a jitter component, we are able to achieve **1)** a 10x data compression that retains most predictive ability, **2)** 97.3% subject identifiability compared to 62.5% for FC, **3)** a modest 5% AUC classification accuracy improvement, **4)** the ability to create augmentations for contrastive learning, and **5)** the creation of an interpretable method for generating synthetic subject FC based on user-input demographics. It does this without requiring knowledge of a population, as needed by PCA, factor analysis, or deep autoencoders; a single subject is enough. The method is conceptually based on the phase lock value, a concept that was previously widely used in neuroscience, but which does not yield good predictive accuracy. It is especially exciting that this method entangles individual region-region FCs, placing a very useful prior on the generation or decomposition of FC.

### **1.4 Aim 4: Contrastive Learning for Fusing Omics with Brain Imaging**

Modern neuroscience, working at the intersection of brain imaging and cellular/networks level represented by genomics, epigenomics, and transcriptomics, is faced with two main problems and one major opportunity. One of the problems, small sample size and high dimensionality, has been described above. The second problem is the noise inherent in the data and site-specific effects. The major opportunity is the large amount of unlabeled data available from sources such as the UK Biobank and OpenNeuro. This is useful, because, for instance, it has been shown that pretraining on large datasets increases accuracy by 4-6% in the image domain [38]. We plan to leverage the large amount of unlabeled data to increase predictive power, gain appreciation for the commonalities and differences between data sources, and make robust associations between genomics and brain imaging endophenotype.

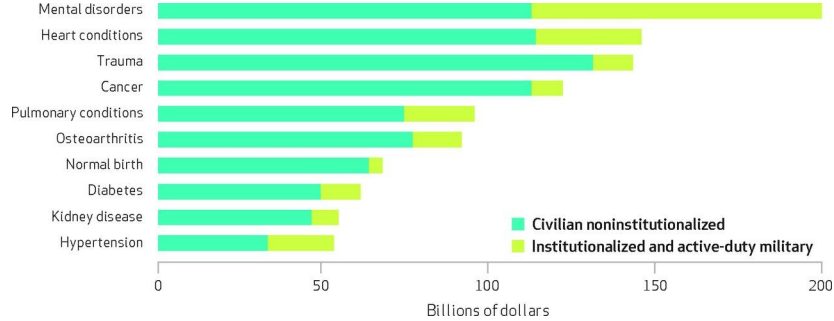


Figure 2: Breakdown of U.S. mental health expenditures. Reproduced from Roehrig [60].

## 2 Background & Significance

### 2.1 Cognitive Science and Mental Illness

Schizophrenia, ADHD, depression, and other mental illness cost the U.S. more than \$201 billion annually [60]. Dementia and Alzheimer's similarly cost the U.S. around \$157 billion annually [32]. Diagnosis of these diseases may be unreliable until symptoms become severe, at which point treatment options may be more expensive (see Figure 2). As an example of prevalence, 1 in 300 people may be affected by schizophrenia [13], 1 in 10 children may be affected by ADHD [15], 1 in 10 people may have had a major depression episode in the past several years [6], 1 in 36 children may be diagnosed with autism spectrum disorder [40], and 1 in 9 Americans over 65 years old are living with Alzheimer's disease [1]. As a representative neurological disease, the biological mechanism of schizophrenia is currently unknown, and while heritability is around 80% [28], only around 23% of variance can be explained by single nucleotide polymorphisms (SNPs) [36]. Indeed, prediction studies using SNP data from the UK Biobank have reported a maximum replicated study AUC of 0.71 [5].

In response to this problem, the National Institutes of Mental Health (NIMH) has developed the Research Domain Criteria (RDoC), which will inform future classification schemes of mental illness [33]. The primary focus of RDoC is on cognitive circuits, with two analysis directions: bottom to top, from cellular function to behavioral responses, and top to bottom, from modes of behavior to molecular/neural wiring that influence phenotypes (see Figure 3). By standing at the interface of phenotype, imaging-based endophenotype, genetics, and multiomics, we seek to untangle the underlying associations and mechanisms with a potential for high impact in the field.

### 2.2 fMRI and Functional Connectivity

Functional magnetic resonance imaging (fMRI) provides a non-invasive estimate of brain activity by exploiting the blood oxygen level-dependent (BOLD) signal

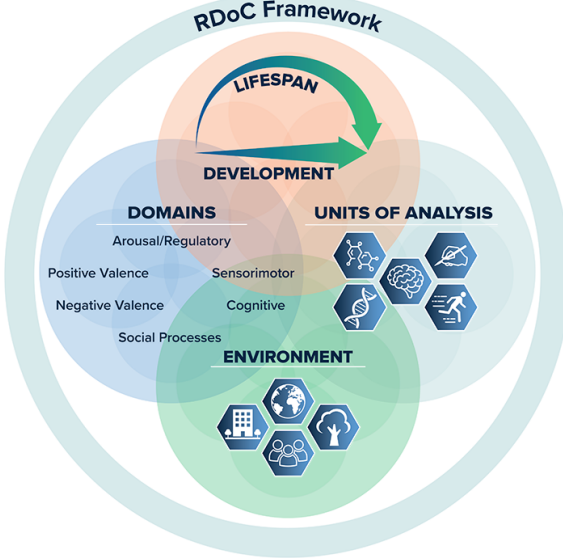


Figure 3: RDoC is a research framework for studying cognition and cognitive pathology. By investing in this model, the NIMH hopes to better understand, diagnose, prevent, and cure psychiatric illness.

[3]. This high-acuity imaging data can be used to predict variables like age, sex, intelligence, and disease status [46][82][56][16]. Interestingly, the gap between fMRI-predicted brain age and biological age can identify Alzheimer’s disease patients prior to the onset of symptoms [42]. Early work in fMRI utilized statistical techniques on voxel intensities to measure brain region activation and group differences [44]. Meanwhile, functional connectivity (FC), the temporal Pearson correlation between brain regions, is more common in predictive studies [23]. An example of the pipeline for processing fMRI data is shown in Figure 4. One potential problem with voxel-based fMRI analysis is the poor test-retest replicability, the majority of studies having an intraclass correlation coefficient of only 0.397 [18]. It is perhaps for this reason that FC-based analysis has become more popular. Interestingly, FC has even been used for mechanistic studies of aggression in response to olfactory stimulus [43], the traditional province of statistical fMRI techniques.

One of the main problems with fMRI studies is small sample size combined with high feature dimensionality. Studies with small sample size only have the power to detect very large effects. Many effects that are found in small studies may be due to noise. When identifying regions that are associated with in-scanner tasks, it was found that the average minimum cohort size needed to reproducibly identify the same region 50% of the time in independent samples was  $N=36$  [72]. In contrast, models deployed clinically use thousands of subjects

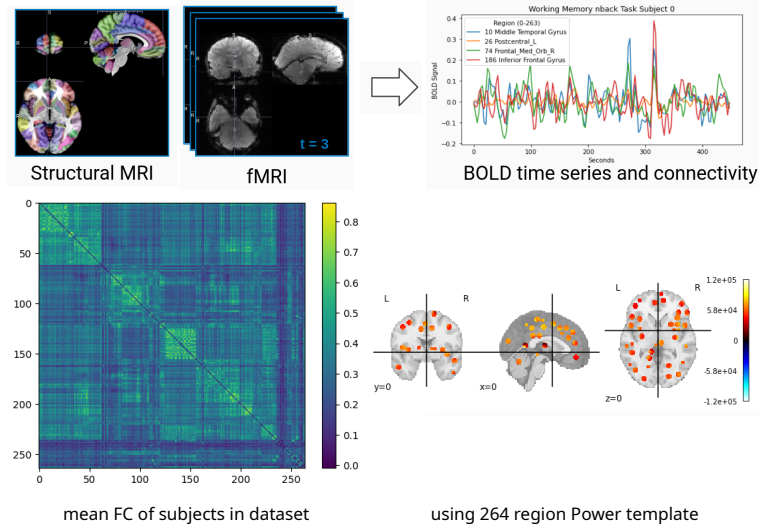


Figure 4: An example of conversion of fMRI BOLD data into functional connectivity (FC). Regions are delineated using either a template or independent component analysis (ICA) [8]. The ROIs in this figure are created using the Power template [54], the 264 regions of which belong to approximately 14 functional networks (see Table 1).

### Functional Networks

ROIs		ROIs	
0-29	Somatomotor Hand	156-180	Frontoparietal
30-34	Somatomotor Mouth	181-198	Salience
35-48	Cinguloopercular	199-211	Subcortical
49-61	Auditory	212-220	Ventral Attention
62-119	Default Mode	221-231	Dorsal Attention
120-124	Memory	232-235	Cerebellar
125-155	Visual	236-263	Uncertain

Table 1: Partition of regions into brain networks in the Power template[54].

for training and validation [62]. In 2017 and 2018, the median cohort sizes for published experimental and clinical MRI studies were 23 and 24 subjects, respectively, and less than 1% of the 272 papers surveyed reported cohort sizes greater than 100 [68]. This may be attributed to both cost, at \$500-\$1000 per subject, and the difficulty of collecting the data, stemming from long scan times, subject discomfort in the scanner, and experimental design [68].

Besides the small sample size of fMRI studies, the effect sizes being measured are also quite small. For example, Bennett et al. [4] found that many effects found as marginally significant by standard analysis are simply due to noise or faulty statistical practices [39]. Additionally, changes in either scanner parameters [63] or preprocessing pipeline [14] may result in large changes in FC or predictive capability. As an example of small effect size, we take the example of intelligence prediction. Many studies have used FC features to predict intelligence, explaining 10% of the variance in a population [47] or achieving a small correlation with ground truth of  $\rho \approx 0.3$ . [53] We show, however, that the FC feature to intelligence correlation is probably due to a confounding effect of race on FC. Indeed, previous studies have shown that AI models can sometimes trivially detect and be confounded by race. [21] In this work, we find that the race confound affects connectivity data, that is, FC can be easily used to predict race.

### 2.3 Decompositions and Generative Models

Since our Aim 3 includes the creation of a generative model and decomposition for FC, we include a review of commonly used decomposition methods. Traditional methods include (probabilistic) principal component analysis (PCA), factor analysis (FA), and canonical correlation analysis (CCA) [45][66]. Deep autoencoders may also be used [45]. However, these are linear methods, or, in the case of autoencoders, specific to a particular framework, and fail to take into account important non-linear effects, as found in, e.g., dynamically changing transcriptomics data. To remedy this, the t-stochastic neighbor embedding (t-SNE) [73] and uniform manifold approximation (UMAP) [41] and projection methods have been developed and are widely used. Even these methods, however, have been shown to be inferior when applied to temporal data, and the learnable latent embeddings for neural analysis model (CEBRA) has been created to fill an unmet need [65] (see Figure 5). Dynamic FC has been shown to be superior to FC in some cases, in one study resulting in a 30% improved prediction of schizophrenia diagnosis [58], although other studies report a more modest benefit [35]. In any case, all of these methods require knowledge of a population to perform latent space transformation, while in our case the decomposition only requires a single subject.

In terms of generative models, Zhao et al. [81] and others [37] have used GANs to help discriminate between patients and healthy controls. Tan et al. [71] have used a manifold-regularized Wasserstein distance GAN to achieve modest prediction gains. However, these GAN-based methods fail to model the underlying time-varying BOLD signal that underpins FC. Therefore they cannot be

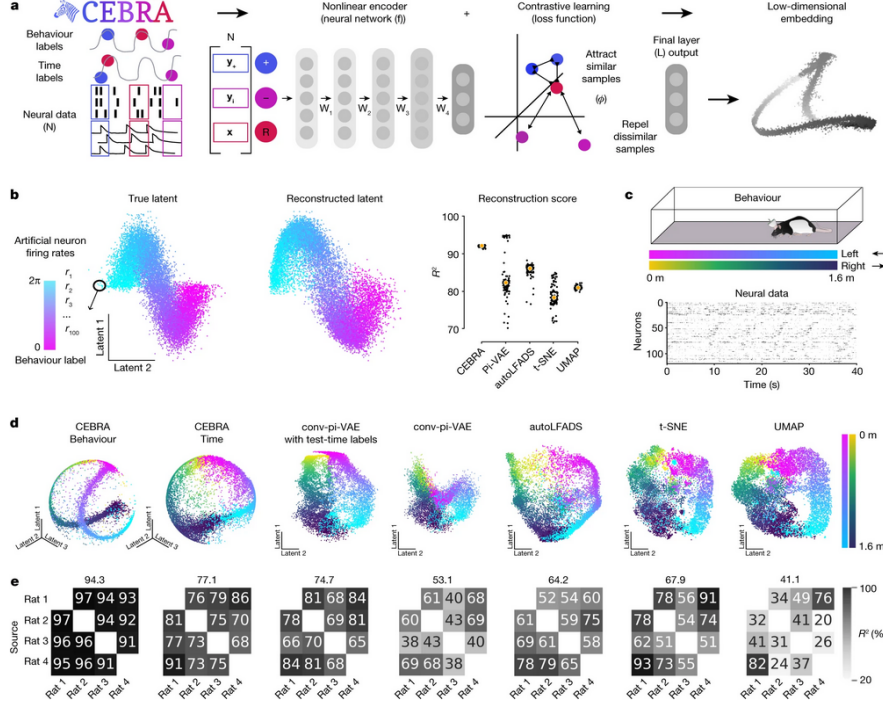


Figure 5: Example of the superior latent variables generated by CEBRA, which takes into account temporal information, compared to t-SNE and UMAP, which do not. Reproduced from Schneider et al. [65].

used for decomposition, dimensionality reduction, or easy interpretation as can our work (see Section 3.3).

It should be noted that the field is also concerned with identifying causal, rather than correlational effects from brain imaging data [59]. In contrast to static or dynamic FC, which only measure correlations, effective connectivity measures the causal influence of one brain region on another [29]. Effective connectivity can be measured using Granger Causality [29] or Transfer Entropy [51], with both approaches providing information complementary to FC. Indeed, the concept of dynamic effective connectivity has been proposed by Friston and uses the process of spectral dynamic causal modeling (spDCM) to estimate connection strength [52]. Dynamic causal modeling (DCM) [27][61] and structural equation modeling (SEM) [76] approaches are important because they provide a neurological model for the flow of information in the brain, with the downside that they are computationally expensive. Indeed, our group has extensive experience applying efficient directed graphical models to the study of both normal development [30] and psychiatric disorders [79]. We have also begun the deep collaborative study of the interaction between brain regions and genomics [31].

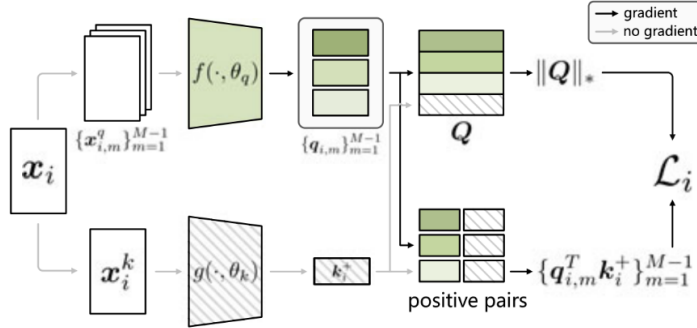


Figure 6: Conceptual framework of the contrastive learning model LORAC utilizing a low-rank promoting prior on the matrix  $\mathbf{Q}$ . Such low-rank priors can serve to de-noise the complex neural signal in fMRI and recover the true features. Reproduced from Wang et al. [75].

We note, however, that even since the days of ANOVA-based statistical methods, fMRI has suffered from a reproducibility crisis [4][17]. Therefore a focus on simplicity and reproducibility [72] may be preferred.

## 2.4 Contrastive Learning and Data Fusion

Our plan for Aim 4 is to combine brain imaging data with contrastive learning to leverage the large amount of data available from projects such as the UKB, which has close to 50,000 patients with fMRI scans [67]. This is useful because the cost of acquiring scans of a single patient with disease of interest is large, ranging from \\$500-\\$1000 [69]. To overcome this financial burden, we will leverage the large amounts of publicly fMRI data available, e.g, from the UKB [67] and OpenNeuro.<sup>1</sup>

Contrastive learning is a form of metric learning which identifies commonalities between data points in a self-supervised manner using the concepts of positive and negative samples [20]. There are many frameworks available for contrastive learning, based around momentum encoders (MoCo) [26], stop gradient operations (SimSiam) [11], data augmentations (SwAV) [10], or maximizing correlation (BarlowTwins) [77]. The promise of these frameworks is that they surpass supervised pre-training in terms of accuracy on image datasets [10]. Recently, contrastive learning has been combined with a low-rank approximation (LORAC) to achieve unprecedented levels of classification accuracy [75]. This is promising for study of the connectome/chronnectome because the connectivity matrices may be approximated by low-rank signal corrupted by noise. The conceptual model of LORAC is reproduced in Figure 6. A model incorporating contrastive learning of images and genomics, called ContIG, has achieved

<sup>1</sup><https://openneuro.org/>

state of the art results on using retinal images and gene sequencing to diagnose Diabetic Retinopathy [70].

Our goal is to both identify scientifically important associations and to create models and tools for use by others. We have already completed several aims and created several tools with this goal in mind (Latent Similarity, ImageNomer, and AngleBasis). By finding interesting associations between imaging endophenotype and multiomics, along with use of large open datasets such as OpenNeuro (see Footnote 1) or the UKB [67], we hope to move the field forward on both the scientific and clinical axes.

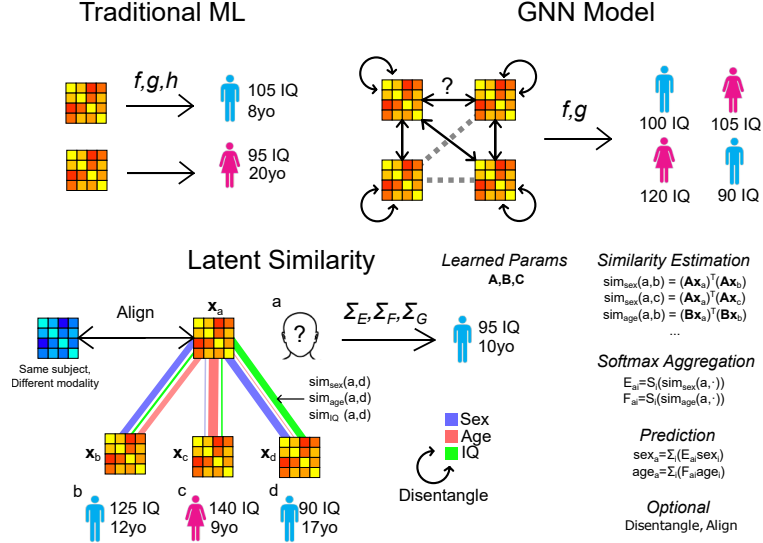


Figure 7: An overview of our Latent Similarity model [47]. In traditional machine learning, estimation of response variables is decoupled from inter-subject similarity, whereas GNN models require additional degrees of freedom to estimate edges between subjects. Our model calculates similarity between subjects based on a set of response variables and incorporates multi-modal feature alignment (in addition to ensembling) as well as sparsity and feature disentanglement. Downloadable tool is available at <https://github.com/aorliche/LatentSimilarity>.

### 3 Research Project Description

#### 3.1 Aim 1: Latent Similarity Identifies Important Functional Connections for Phenotype Prediction

In **Aim 1** we seek to identify robust group differences in the static connectome and create tools for data exploration. We leverage a CCA-like design [66] based on kernel learning to construct a subject-subject similarity graph using a low dimensional kernel projection:

$$\begin{aligned} \text{sim}(a, b) &= \langle \phi(\mathbf{x}_a), \phi(\mathbf{x}_b) \rangle \\ &= \mathbf{x}_a \mathbf{A} \mathbf{A}^T \mathbf{x}_b^T, \end{aligned} \tag{1}$$

where  $\mathbf{A} \in \mathbb{R}^{d \times d'}$  is the kernel matrix and  $\mathbf{x}_a, \mathbf{x}_b \in \mathbb{R}^d$  are feature vectors for subjects  $a$  and  $b$ , respectively. These similarities are then adjusted by passing them through a softmax activation function while masking each subject's self-similarity. The entire model for a single predictive task and a single fMRI paradigm is as follows:

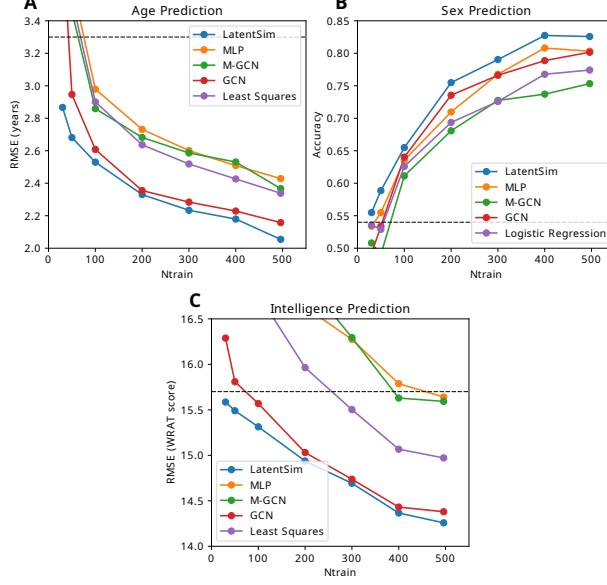


Figure 8: Results of the superior predictive ability of LatSim compared to traditional linear, deep, and graph neural network machine learning models. Dashed black line represents the null model.

$$\begin{aligned}
 \mathbf{M} &= \text{diag}(\infty), \\
 \mathbf{E} &= S_{Row}((\mathbf{1} - \mathbf{M}) \odot \mathbf{X} \mathbf{A} \mathbf{A}^T \mathbf{X}^T), \\
 S(\mathbf{z})_i &= \frac{e^{z_i/\tau}}{\sum_{j=0}^N e^{z_j/\tau}}, \tag{2}
 \end{aligned}$$

where  $\mathbf{E} \in \mathbb{R}^{N \times N}$  is the final similarity matrix,  $\mathbf{M} \in \mathbb{R}^{N \times N}$  is a mask to remove self-loops in predictions,  $\infty \in \mathbb{R}^N$  is a vector of infinite-valued elements,  $\mathbf{1} \in \mathbb{R}^{N \times N}$  is a matrix of ones,  $\mathbf{X} \in \mathbb{R}^{N \times d}$  is the feature matrix,  $\mathbf{A} \in \mathbb{R}^{d \times d'}$  is the kernel taking connectivity features to a lower latent dimension,  $N$  is the number of subjects,  $d$  is the number of features (FCs),  $S(\mathbf{z})_i$  is the softmax function with temperature  $\tau$ , and  $S_{Row}(\mathbf{Z})$  is a function applying softmax to each row of the input matrix. High or low temperature  $\tau$  determines whether the subject-subject similarity matrix  $\mathbf{E}$  is more dense or sparse, respectively.

The overall Latent Similarity model is presented in Figure 7. Using the Latent Similarity model results in superior predictive ability, especially at small sample sizes, compared to traditional linear, deep, and graph neural network models, as seen in Figure 8.

Additionally, we use LatSim in the inner loop of a greedy feature selection algorithm. The greedy selection process works on a combination of iterative estimation, bootstrap ensembling, and next feature selection by linear correlation

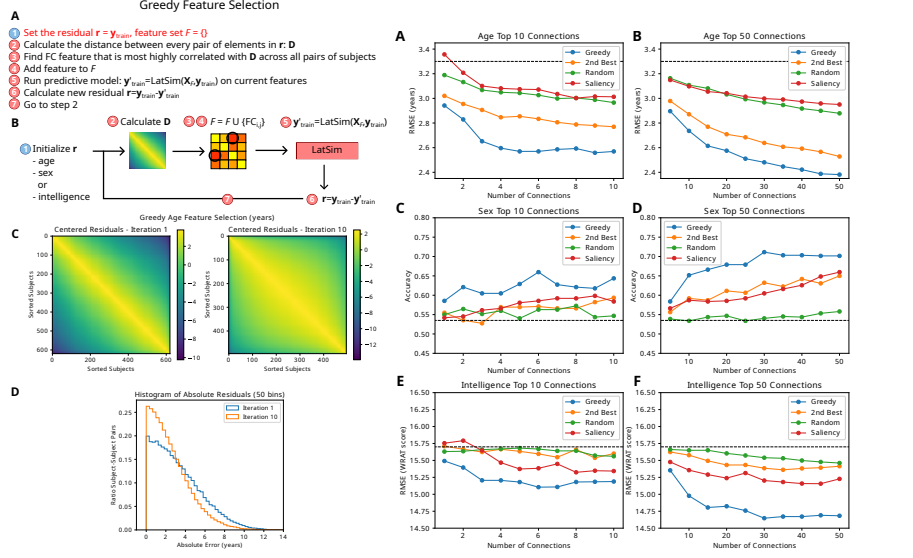


Figure 9: Left: flowchart and description of the greedy feature selection algorithm. Right: prediction accuracy for features chosen using greedy selection, 2nd best greedy selection, random features, or saliency (gradient-based) features.

with residual. See Figure 9 for an overview of the algorithm. We find greedy selection results in superior feature selection for each of age, sex, and intelligence prediction compared to 2nd best features, random features, or saliency (gradient-derived) features, as seen in Figure 9. Finally, some of the most prominent regions taking part in connections important for prediction are plotted on top of a glass brain in Figure 10. It should be noted that, although there are only a few best features, the 2nd best features are not that far off, due to the large amount of redundant or semi-redundant information present in FC.

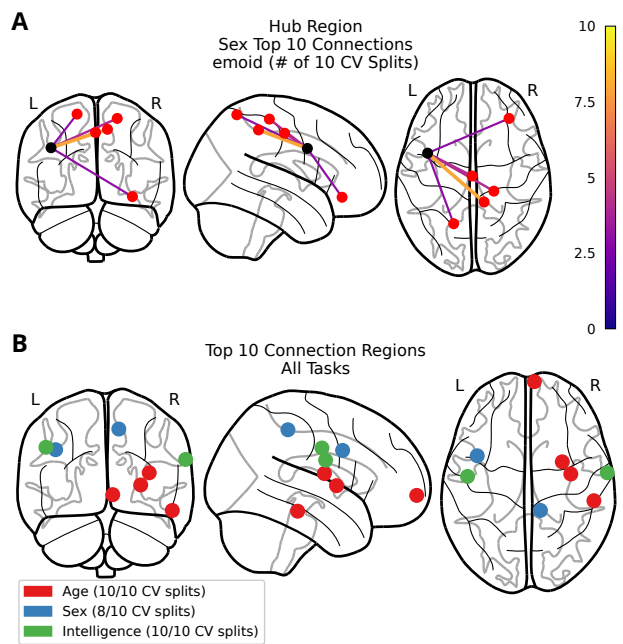


Figure 10: Top regions participating in FCs for age, sex, and intelligence prediction selected by greedy selection. Although these are the optimal features, many next-best features exist.

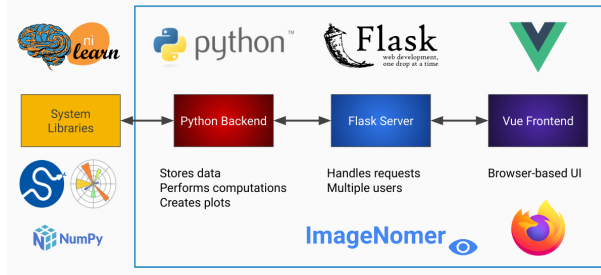


Figure 11: The ImageNomer architecture, listing component modules. Preprint available online [49][48] and code available at <https://github.com/TulaneMBB/ImageNomer>.

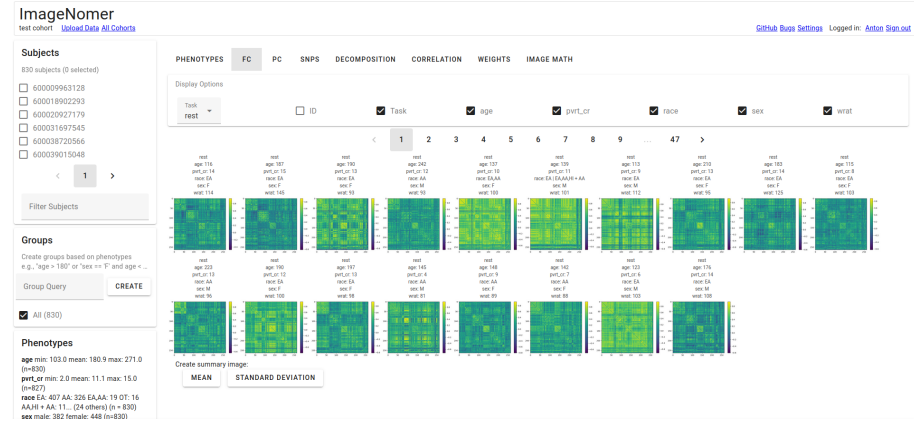


Figure 12: Main view of ImageNomer, showing distribution of subject connectivities (able to display FC, partial correlation, or other connectivity measures). On-line demo available at <https://aorliche.github.io/ImageNomer/live/>

### 3.2 Aim 2: ImageNomer: developing an fMRI and omics visualization tool to detect racial bias in functional connectivity

Our goal in **Aim 2** was to create a tool for the fast and efficient exploration of large datasets. Our tool, called ImageNomer (see Figures 11 and 12), is able to display subject FCs from a dataset, create subgroups, find correlations in demographic features, and identify confounders. During the creation of ImageNomer, we tested the software with models to predict age, sex, race, and Wide Range Achievement Test score in the Philadelphia Neurodevelopmental Cohort (PNC) dataset. We found that WRAT score prediction is confounded with race, and when predicting within-race the ability to predict achievement disappears. The PNC dataset consists of 1,500 normal children with fMRI scans 8-22 years old.

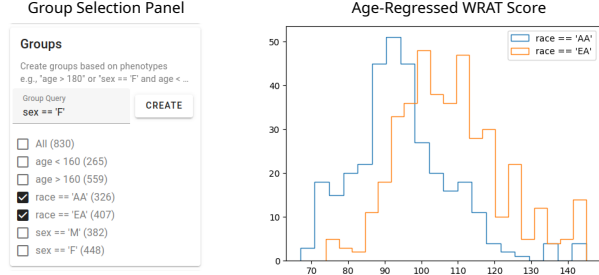


Figure 13: Visualization of the race confound in the PNC dataset for WRAT score prediction using ImageNomer.

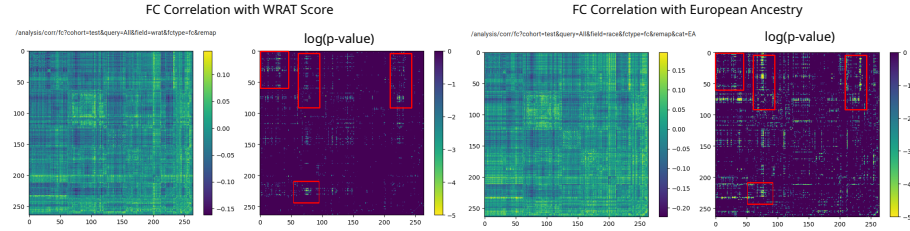


Figure 14: We see that correlation of FC with achievement (as measured by WRAT computerized battery [64]) is a subset of FC correlation with race, leading to the conclusion that we are measuring a confound influenced by ethnicity difference or possibly socio-economics.

We extended our analysis to the BSNIP dataset of schizophrenics, relatives, and normal controls, and found that the race prediction signal is one of the strongest signals, i.e. it is an important and large confound.

Part of our abstract is reproduced below: We find that FC features can be used to predict race with 85% accuracy, compared to 78% accuracy for sex prediction. We also find that 10 features can predict race with up to 72% accuracy, while sex prediction at 10 features is not reliable. For comparison, age is the phenotype most amenable to prediction, with 35% of variance in age explained by the full model and 15% of variance explained by 10 features. We perform a validation study using the Bipolar and Schizophrenia Network for Intermediate Phenotypes (BSNIP) dataset. We find a race prediction accuracy of 79% in BSNIP, and an average 66% and 68% race prediction accuracy when transferring models between PNC and BSNIP. Using ImageNomer, this work finds that race can be robustly predicted by FC. Additionally, it casts doubt on the possibility of finding unbiased achievement-related features in fMRI and SNPs of healthy adolescents.

We show the race confound visible in the PNC dataset displayed in ImageNomer in Figure 13. We show the overlap of FC correlation with race and WRAT score in Figure 14. A summary of our main finding is shown in Figure 15.

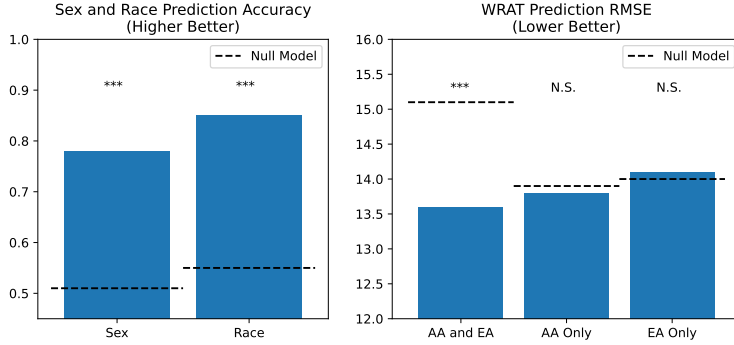


Figure 15: We see robust sex and race prediction in the PNC cohort, as well as in WRAT score prediction in mixed groups. Ability to predict achievement disappears when predicting in racially homogenous groups.

### 3.3 Aim 3: Angle Basis: A Generative Model and Decomposition for Functional Connectivity

In our experiments on the chronnectome and dynamic dictionary learning (accepted at OHBM 2023 but not included in the main body of this prospectus, see Appendix A), we found a very parsimonious and theoretically motivated representation of FC. This makes up our **Aim 3**. Traditional decomposition like PCA or Factor Analysis rely on finding dictionary entries based on commonalities in a population. We find that by using a combination of orthogonal sine waves and a jitter component, we are able to reconstruct most of the information in the FC using around 10% of the number of variables, and requiring only the FC of one subject as input. The decomposition is motivated by the Hilbert transform and the widely-studied but relatively poor for prediction Phase Lock Value (PLV) [22][34]:

$$\begin{aligned}
 H[x](t) &= \frac{1}{\pi} \text{p.v.} \int_{-\infty}^{\infty} \frac{x(\tau)}{t - \tau} d\tau \\
 x_a(t) &= x(t) + iH[x(t)] \\
 x_a(t) &= a(t)e^{i\theta(t)} \\
 \theta_{cd}(t) &= \theta_c(t) - \theta_d(t) \\
 \text{PLV}_{cd} &= \frac{1}{T} \left| \sum_{t=1}^T e^{i\theta_{cd}(t)} \right|
 \end{aligned} \tag{3}$$

Here  $x(t)$  is the original time-dependent BOLD signal at one ROI, and the subscripts  $c, d$  refer to different ROIs. We use a simpler but more robust model to decompose the FC into a basis of orthogonal sine waves and jitter component:

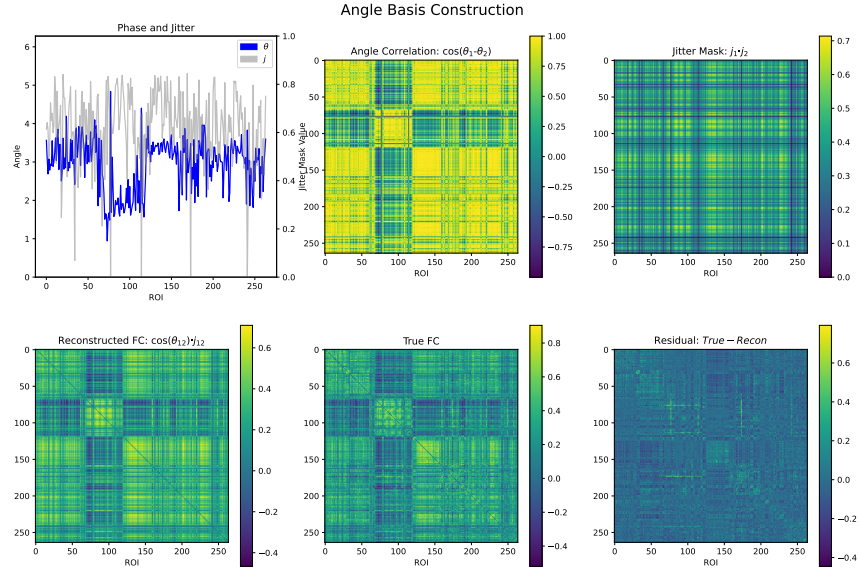


Figure 16: Example of the angle basis reconstruction of one representative subject from the PNC dataset. The prominent block corresponds to the default mode network (DMN). The scan is probably of a female, due to the high within-DMN connectivity [19]. Here only one basis is used. The AngleBasis tool [50] and generative model are available at <https://github.com/aorliche/AngleBasis>.

$$\begin{aligned} \hat{\rho}_{cd}^{(n)} &= j_c^{(n)} \cdot j_d^{(n)} \cdot \cos(\theta_c^{(n)} - \theta_d^{(n)}) \\ \tilde{\rho}_{cd} &= \frac{1}{N} \sum_{n=1}^N \hat{\rho}_{cd}^{(n)} \end{aligned} \quad (4)$$

where  $\rho_{cd}$ ,  $\tilde{\rho}_{cd}$  are the true and estimated FC values, respectively. An example decomposition is shown in Figure 16.

Using the residual of the decomposition results in a 97.3% subject identifiability, compared to 62.5% for FC (see Figure 17). Using the ensemble of reconstruction and residual, we show in Table 2 that we are able to achieve a modest classification improvement across the board.

One of the more exciting uses of this model is the ability to generate a distribution of FCs for synthetic subjects which are compatible with patient phenotypes. This can help visualize what a representative FC for a patient population might look like, and may help give intuition for working with FC.

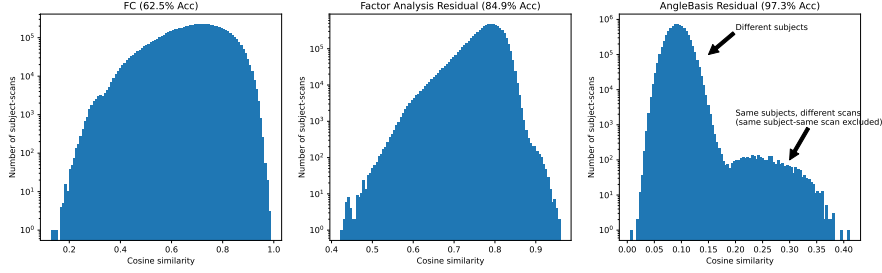


Figure 17: Identification of subjects from different scans in the PNC dataset. Histograms show the number of scan pairs at a particular cosine similarity value. One can clearly identify scans of the same subject in the angle basis residual, but not as much using FC or Factor Analysis. Most subjects in the PNC dataset contain 3 scans with different in-scanner tasks. A total of 3849 scans were used.

Table 2: Classification Accuracy (AUC)

Dataset	Predictive Task	FC	Deep AE Ens	AB+Res Ens	p-value
BSNIP	SZ/NC	$0.785 \pm 0.048$	$0.701 \pm 0.062$	<b><math>0.804 \pm 0.040</math></b>	0.240
BSNIP	Sex	$0.755 \pm 0.023$	$0.645 \pm 0.085$	<b><math>0.791 \pm 0.022</math></b>	0.002
BSNIP	Race	$0.845 \pm 0.022$	$0.739 \pm 0.051$	<b><math>0.866 \pm 0.023</math></b>	0.108
PNC	Sex	$0.886 \pm 0.006$	$0.744 \pm 0.065$	<b><math>0.923 \pm 0.010</math></b>	< 0.001
PNC	Race	$0.946 \pm 0.007$	$0.812 \pm 0.040$	<b><math>0.973 \pm 0.003</math></b>	< 0.001
BSNIP→PNC	Sex	$0.667 \pm 0.017$	$0.601 \pm 0.032$	<b><math>0.700 \pm 0.013</math></b>	< 0.001
BSNIP→PNC	Race	$0.807 \pm 0.018$	$0.710 \pm 0.010$	<b><math>0.847 \pm 0.012</math></b>	< 0.001
PNC→BSNIP	Sex	$0.629 \pm 0.019$	$0.572 \pm 0.019$	<b><math>0.667 \pm 0.013</math></b>	< 0.001
PNC→BSNIP	Race	$0.800 \pm 0.010$	$0.702 \pm 0.022$	<b><math>0.832 \pm 0.009</math></b>	< 0.001

For instance, we show sample generated FCs for two subjects in Figure 18 and group differences in Figure 19.

To reiterate, AngleBasis offers the following advantages complementary to FC:

1. More than 10x data compression
2. 97.3% subject fingerprinting identification, compared to 62.5% for FC
3. Modest classification AUC improvement of 5% compared to FC
4. Possibility for data augmentation
5. Generation of synthetic FC based on scalar patient phenotype/clinical characteristics, including a view of the distribution of possible FCs (helps greatly with interpretability/explainability)
6. Does not require knowledge of a population; a single subject is enough

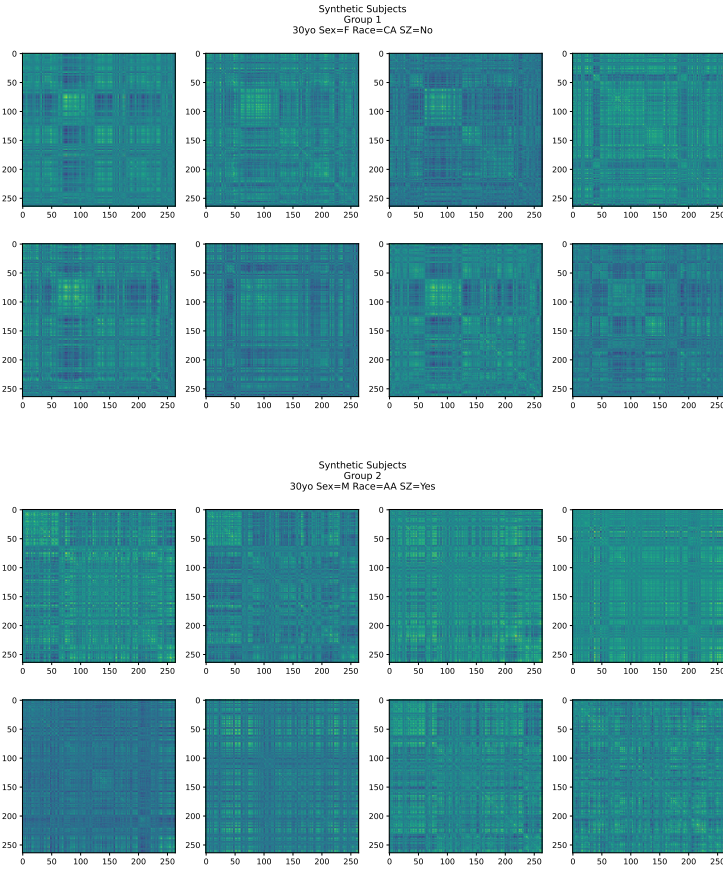


Figure 18: First 8 synthetic subjects from 30yo normal CA female group and 30yo schizophrenic AA male group.

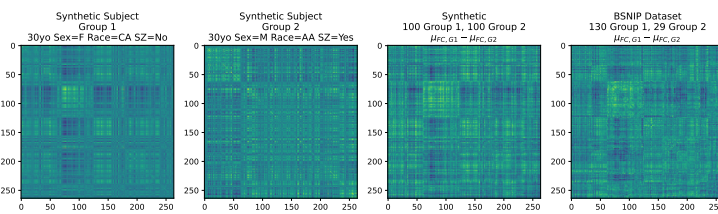


Figure 19: Difference between the mean of synthetic subject groups is almost exactly the same as between corresponding real subject groups.

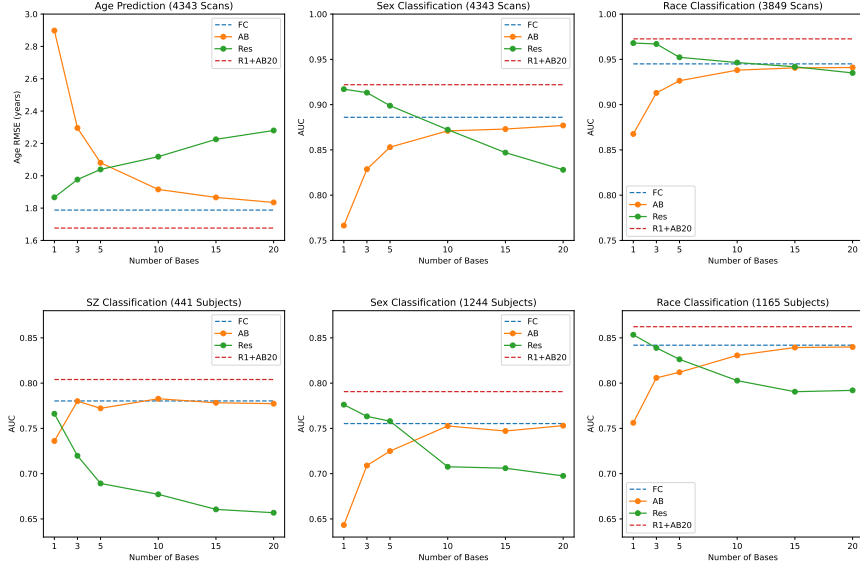


Figure 20: The prediction fidelity (RMSE and AUC) of the angle basis reconstruction and residual as a function of the number of bases. Top plot is for the PNC dataset, bottom is for the BSNIP dataset.

Both the angle basis decomposition and its residual have approximately equal predictive ability, the proportion changing inversely as the number of basis sinusoids and jitter masks increases. The relationship is shown in a graph for the PNC (Philadelphia Neurodevelopmental Cohort) and BSNIP (Bipolar and Schizophrenia Network for Intermediate Phenotypes) datasets in Figure 20.

### 3.4 Aim 4: Contrastive Learning for Fusing Omics with Brain Imaging

In **Aim 4** we move from uni-modal analysis of fMRI data to multi-modal analysis of fMRI and omics data using contrastive learning. Contrastive learning is an important new paradigm for leveraging large amounts of unlabeled data. It has been shown to create more robust models [57].<sup>2</sup> The basic concept is to use data augmentation or other strategies to create positive and negative pairs from a learned representation function. These robust representations may then be used in downstream tasks. The classic InfoNCE loss used to train contrastive learning models is given below:

$$\mathcal{L}_{CL} = -\frac{1}{N} \sum_i^N \log \frac{e^{\mathbf{q}_i^T \mathbf{k}_i^+ / \tau}}{e^{\mathbf{q}_i^T \mathbf{k}_i^+ / \tau} + \sum_{j=1}^K e^{\mathbf{q}_i^T \mathbf{k}_{i,j}^- / \tau}} \quad (5)$$

The elements of the equation are as follows:

- $\mathbf{q}_i$  is an image  $\mathbf{x}_i$  mapped into a query latent via a query encoder  $\mathbf{q}_i = f(\mathbf{x}_i)$  The goal of contrastive learning is to learn  $f(\cdot)$
- $\mathbf{k}_i$  is an image mapped into a key latent via a key encoder  $g(\mathbf{x}_i)$  (+ and – are positive and negative samples)
- $N$  is the batch size
- $K$  is the number of negatives per positive sample
- $\tau$  is a temperature determining how peaked or flat the Softmax function is

Recently, Wang et al. [75] have created a low rank version of contrastive learning in the image domain with the idea that important features should lie on a low dimensional manifold. They modify Equation 5 to contain a low rank-promoting prior based on a nuclear norm approximation to matrix rank:

$$\begin{aligned} \mathcal{L}_i &= -\frac{1}{M-1} \sum_m^{M-1} \log \frac{e^{\mathbf{q}_{i,m}^T \mathbf{k}_i^+ / \tau} \cdot h(\mathbf{Q})}{e^{\mathbf{q}_{i,m}^T \mathbf{k}_i^+ / \tau} \cdot h(\mathbf{Q}) + \sum_{j=1}^K e^{\mathbf{q}_{i,m}^T \mathbf{k}_{i,j}^- / \tau}} \\ \mathcal{L} &= \frac{1}{N} \sum_i^N \mathcal{L}_i \end{aligned} \quad (6)$$

where  $h(\mathbf{Q})$  is the low-rank promoting prior based on a Laplace distribution. It uses the nuclear norm of the matrix  $\mathbf{Q}$  comprised of stacked views of the positive samples and a tunable hyperparameter  $\beta$ , shown below:

$$h(\mathbf{Q}) = e^{-\frac{\|\mathbf{Q}\|_*}{M \cdot \beta \cdot \tau}} \quad (7)$$

---

<sup>2</sup><https://openai.com/research/clip>

As mentioned in Section 2.3, Schneider et al. [65] created a contrastive learning paradigm with neural-network based similarity function  $\psi(\mathbf{x}, \mathbf{y}) = \phi(\mathbf{f}(\mathbf{x}), \mathbf{f}'(\mathbf{y}))$  extended with temporal information to produce embeddings. These embeddings were for rat neuron spiking data  $\mathbf{x}$  in an environment with continuous outcomes  $\mathbf{y}$  (see Figure 5). Their objective function to be minimized was as follows:

$$\mathbb{E}_{\mathbf{x} \sim p(\mathbf{x}), \mathbf{y}_+ \sim p(\mathbf{y}|\mathbf{x}), \mathbf{y}_i \sim q(\mathbf{y}|\mathbf{x})} \left[ -\psi(\mathbf{x}, \mathbf{y}_+) + \log \sum_{i=1}^N e^{\psi(\mathbf{x}, \mathbf{y}_i)} \right] \quad (8)$$

Our sister group at Tulane from the School of Medicine and Department of Computer Science has released a study leveraging contrastive learning and transformer self-attention [74] to achieve superior multi-omics integration [80]. We hope to extend their framework with our own knowledge of static and dynamic fMRI-based imaging features to gain further insight into both normal and abnormal cognition.

An additional purpose of **Aim 4** is to transfer the tools created and knowledge acquired in the first three aims into a clinical setting, to help address some of the \$200 billion dollar burden of mental health and neuro-degenerative illness in the U.S. [60][32]. As a first step, we want to create tools used by other researchers. Examples of widely used and important tools developed by other labs include PLINK [55] and Seurat [25], for single-nucleotide polymorphism (SNP) analysis and omics integration, respectively. In the neuroimaging and neuroscience field, our collaborators at Georgia Tech have released the Matlab-based Group ICA of fMRI Toolbox (GIFT) and Fusion ICA Toolbox (FIT).<sup>3</sup> These tools utilize a graphical user interface, shown in Figure 21. The same group has also released source code for estimation of window-based dynamic FC (dFC).

An almost indispensable tool for neuroimaging research is SPM12, also Matlab-based.<sup>4</sup> A downside of some of these tools is that Matlab is tied to a paid license. In terms of libraries for programmer use, an example of a best-in-class package is the cca-zoo<sup>5</sup> Python package, containing more than 20 variants of different implementations of CCA (see, e.g., Andrew et al. [2]). An additional example of resources we are excited to integrate with are public-access data or tool repositories, examples of which are OpenNeuro<sup>6</sup> and Nemar.org [12],<sup>7</sup> respectively. Our goal is that our models should be robust on multiple datasets and easy to use for researchers and clinicians alike. Although this is our last aim, several tools have already been created by us and are publicly available (see Sections 3.1, 3.2, and 3.3).

---

<sup>3</sup><https://trendscenter.org/software/gift/>

<sup>4</sup><https://www.fil.ion.ucl.ac.uk/spm/software/spm12/>

<sup>5</sup><https://cca-zoo.readthedocs.io/en/latest/>

<sup>6</sup><https://openneuro.org/>

<sup>7</sup><https://nemar.org/>

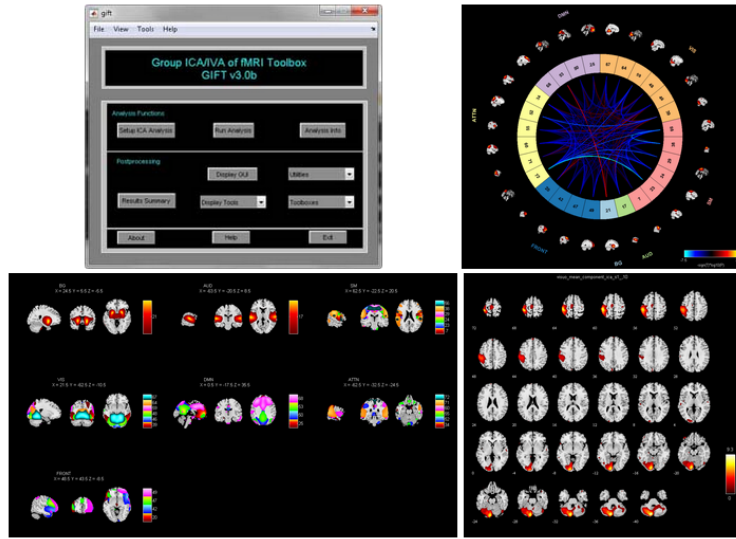


Figure 21: Screenshot of the Matlab-based GIFT and FIT tools from our collaborators at Georgia Tech. Reproduced from footnote 3.

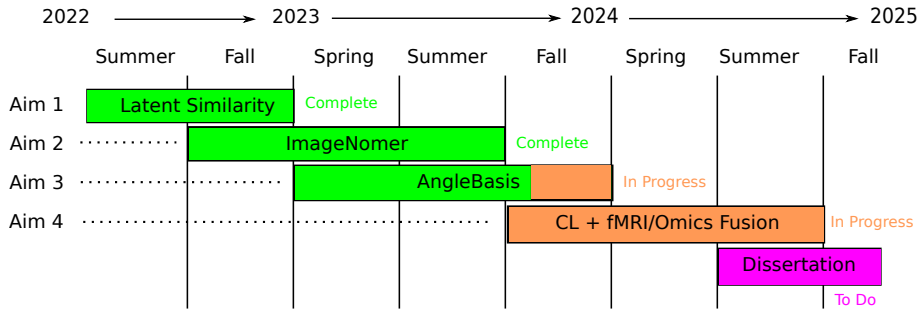


Figure 22: Aims and projected timeline for dissertation research.

## 4 Timeline

### 4.1 Fall 2022: Aim 1 - Latent Similarity

Create graphical Latent Similarity model to identify inter-group differences in small sample size, high dimensionality datasets. Publish an easy to use programming interface downloadable by other scientists. Status: **complete**.

### 4.2 Spring 2023: Aim 2 - ImageNomer

Create the ImageNomer software tool for exploring imaging datasets, clinical variables, and genomics. Create tools for interpretation of both deep and shallow machine learning models and the identification of data correlations. Status: **complete**.

### 4.3 Fall 2023: Aim 3 - Angle Basis

Create a generative model of FC that allows for increased identifiability, data compression, and increased predictive performance. Create synthetic data and augmentations as a prelude to using contrastive learning for studying the interactome. Status: **in progress**.

### 4.4 Spring 2024: Aim 4 - Contrastive Learning and Omics Fusion

Extend the low-rank contrastive learning work of [75] to brain dynamics, genomics, and cognitive phenotypes, to uncover neural correlates of behavior in a data-driven manner. Status: **in progress**.

### 4.5 Fall 2024: Dissertation

Combine previous work on easy to use tools; begin and complete dissertation document. Status: **to do**.

## References

- [1] 2023 alzheimer’s disease facts and figures. *Alzheimers. Dement.*, 19(4):1598–1695, Apr. 2023.
- [2] G. Andrew, R. Arora, J. Bilmes, and K. Livescu. Deep canonical correlation analysis. In S. Dasgupta and D. McAllester, editors, *Proceedings of the 30th International Conference on Machine Learning*, volume 28 of *Proceedings of Machine Learning Research*, pages 1247–1255, Atlanta, Georgia, USA, 17–19 Jun 2013. PMLR. URL <https://proceedings.mlr.press/v28/andrew13.html>.
- [3] J. W. Belliveau et al. Functional mapping of the human visual cortex by magnetic resonance imaging. *Science*, 254:5032:716–9, 1991.
- [4] C. M. Bennett, M. B. Miller, and G. L. Wolford. Neural correlates of interspecies perspective taking in the post-mortem atlantic salmon: An argument for multiple comparisons correction. *Neuroimage*, 47(Suppl 1):S125, 2009.
- [5] M. Bracher-Smith, E. Rees, G. Menzies, J. T. R. Walters, M. C. O’Donovan, M. J. Owen, G. Kirov, and V. Escott-Price. Machine learning for prediction of schizophrenia using genetic and demographic factors in the UK biobank. *Schizophr. Res.*, 246:156–164, Aug. 2022.
- [6] D. J. Brody, L. A. Pratt, and J. P. Hughes. Prevalence of depression among adults aged 20 and over: United states, 2013–2016. 2018.
- [7] B. Cai, G. Zhang, A. Zhang, J. M. Stephen, T. W. Wilson, V. D. Calhoun, and Y. ping Wang. Capturing dynamic connectivity from resting state fmri using time-varying graphical lasso. *IEEE Transactions on Biomedical Engineering*, 66:1852–1862, 2019.
- [8] V. D. Calhoun, J. Liu, and T. Adali. A review of group ICA for fMRI data and ICA for joint inference of imaging, genetic, and ERP data. *Neuroimage*, 45(1 Suppl):S163–72, Mar. 2009.
- [9] V. D. Calhoun, G. D. Pearlson, and J. Sui. Data-driven approaches to neuroimaging biomarkers for neurological and psychiatric disorders: emerging approaches and examples. *Curr. Opin. Neurol.*, 34(4):469–479, Aug. 2021.
- [10] M. Caron, I. Misra, J. Mairal, P. Goyal, P. Bojanowski, and A. Joulin. Unsupervised learning of visual features by contrasting cluster assignments. 2020.
- [11] X. Chen and K. He. Exploring simple siamese representation learning. *arXiv preprint arXiv:2011.10566*, 2020.

- [12] A. Delorme, D. Truong, C. Youn, S. Sivagnanam, C. Stirm, K. Yoshimoto, R. A. Poldrack, A. Majumdar, and S. Makeig. NEMAR: an open access data, tools and compute resource operating on neuroelectromagnetic data. *Database*, 2022, 11 2022. ISSN 1758-0463. doi: 10.1093/database/baac096. URL <https://doi.org/10.1093/database/baac096>. baac096.
- [13] P. R. Desai, K. A. Lawson, J. C. Barner, and K. L. Rascati. Estimating the direct and indirect costs for community-dwelling patients with schizophrenia. *J. Pharm. Health Serv. Res.*, 4(4):187–194, Dec. 2013.
- [14] M. N. DeSalvo. Motion-dependent effects of functional magnetic resonance imaging preprocessing methodology on global functional connectivity. *Brain Connect.*, 10(10):578–584, Dec. 2020.
- [15] M. Dinçer, F. S. Uğurtaş Gökçe, H. Gül, Y. Taş Torun, Ş. Bodur, and M. A. Cöngölbaşı. Is processing speed (gs) related to hyperactivity (as a narrow cognitive area of gps): A dimensional approach to heterogeneity of clinical and WISC-IV cognitive profiles in ADHD from RDoC/HiTOP perspective. *J. Atten. Disord.*, 26(13):1747–1761, Nov. 2022.
- [16] Y. Du, Z. Fu, and V. D. Calhoun. Classification and prediction of brain disorders using functional connectivity: Promising but challenging. *Frontiers in Neuroscience*, 12, 2018.
- [17] A. Eklund, T. E. Nichols, and H. Knutsson. Cluster failure: Why fMRI inferences for spatial extent have inflated false-positive rates. *Proc. Natl. Acad. Sci. U. S. A.*, 113(28):7900–7905, July 2016.
- [18] M. L. Elliott, A. R. Knodt, D. Ireland, M. L. Morris, R. Poulton, S. Ramrakha, M. L. Sison, T. E. Moffitt, A. Caspi, and A. R. Hariri. What is the test-retest reliability of common task-functional MRI measures? new empirical evidence and a meta-analysis. *Psychol. Sci.*, 31(7):792–806, July 2020.
- [19] B. Ficek-Tani, C. Horien, S. Ju, W. Xu, N. Li, C. Lacadie, X. Shen, D. Scheinos, T. Constable, and C. Fredericks. Sex differences in default mode network connectivity in healthy aging adults. *Cereb. Cortex*, Dec. 2022.
- [20] B. Ghajogh, A. Ghodsi, F. Karray, and M. Crowley. Spectral, probabilistic, and deep metric learning: Tutorial and survey. 2022.
- [21] J. W. Gichoya, I. Banerjee, A. R. Bhimireddy, J. L. Burns, L. A. Celi, L.-C. Chen, R. Correa, N. Dullerud, M. Ghassemi, S.-C. Huang, P.-C. Kuo, M. P. Lungren, L. J. Palmer, B. J. Price, S. Purkayastha, A. T. Pyrros, L. Oakden-Rayner, C. Okechukwu, L. Seyyed-Kalantari, H. Trivedi, R. Wang, Z. Zaiman, and H. Zhang. AI recognition of patient race in medical imaging: a modelling study. *Lancet Digit. Health*, 4(6):e406–e414, June 2022.

- [22] E. Glerean, J. Salmi, J. M. Lahnnakoski, I. P. Jääskeläinen, and M. Sams. Functional magnetic resonance imaging phase synchronization as a measure of dynamic functional connectivity. *Brain Connect.*, 2(2):91–101, June 2012.
- [23] M. D. Greicius, B. Krasnow, A. L. Reiss, and V. Menon. Functional connectivity in the resting brain: A network analysis of the default mode hypothesis. *Proceedings of the National Academy of Sciences*, 100(1):253–258, 2003. doi: 10.1073/pnas.0135058100. URL <https://www.pnas.org/doi/abs/10.1073/pnas.0135058100>.
- [24] D. Hallac, Y. Park, S. Boyd, and J. Leskovec. Network inference via the time-varying graphical lasso. In *Proceedings of the 23rd ACM SIGKDD International Conference on Knowledge Discovery and Data Mining*, New York, NY, USA, Aug. 2017. ACM.
- [25] Y. Hao, S. Hao, E. Andersen-Nissen, W. M. M. III, S. Zheng, A. Butler, M. J. Lee, A. J. Wilk, C. Darby, M. Zagar, P. Hoffman, M. Stoeckius, E. Papalexi, E. P. Mimitou, J. Jain, A. Srivastava, T. Stuart, L. B. Fleming, B. Yeung, A. J. Rogers, J. M. McElrath, C. A. Blish, R. Gottardo, P. Smibert, and R. Satija. Integrated analysis of multimodal single-cell data. *Cell*, 2021. doi: 10.1016/j.cell.2021.04.048. URL <https://doi.org/10.1016/j.cell.2021.04.048>.
- [26] K. He, H. Fan, Y. Wu, S. Xie, and R. Girshick. Momentum contrast for unsupervised visual representation learning. 2019.
- [27] E. Hidalgo-Lopez, P. Zeidman, T. Harris, A. Razi, and B. Pletzer. Spectral dynamic causal modelling in healthy women reveals brain connectivity changes along the menstrual cycle. *Commun. Biol.*, 4(1):954, Aug. 2021.
- [28] R. Hilker, D. Helenius, B. Fagerlund, A. Skytthe, K. Christensen, T. M. Werge, M. Nordentoft, and B. Glenthøj. Heritability of schizophrenia and schizophrenia spectrum based on the nationwide danish twin register. *Biol. Psychiatry*, 83(6):492–498, Mar. 2018.
- [29] P. Hosseinzadeh Kassani, L. Xiao, G. Zhang, J. M. Stephen, T. W. Wilson, V. D. Calhoun, and Y. P. Wang. Causality-based feature fusion for brain neuro-developmental analysis. *IEEE Transactions on Medical Imaging*, 39(11):3290–3299, 2020. doi: 10.1109/TMI.2020.2990371.
- [30] P. Hosseinzadeh Kassani, L. Xiao, G. Zhang, J. M. Stephen, T. W. Wilson, V. D. Calhoun, and Y. P. Wang. Causality-based feature fusion for brain neuro-developmental analysis. *IEEE Trans. Med. Imaging*, 39(11):3290–3299, Nov. 2020.
- [31] W. Hu, X. Meng, Y. Bai, A. Zhang, G. Qu, B. Cai, G. Zhang, T. W. Wilson, J. M. Stephen, V. D. Calhoun, and Y.-P. Wang. Interpretable multimodal fusion networks reveal mechanisms of brain cognition. *IEEE Trans. Med. Imaging*, 40(5):1474–1483, May 2021.

- [32] M. D. Hurd, P. Martorell, A. Delavande, K. J. Mullen, and K. M. Langa. Monetary costs of dementia in the united states. *N. Engl. J. Med.*, 368(14):1326–1334, Apr. 2013.
- [33] T. Insel, B. Cuthbert, M. Garvey, R. Heinssen, D. S. Pine, K. Quinn, C. Sanislow, and P. Wang. Research domain criteria (RDoC): toward a new classification framework for research on mental disorders. *Am. J. Psychiatry*, 167(7):748–751, July 2010.
- [34] J. P. Lachaux, E. Rodriguez, J. Martinerie, and F. J. Varela. Measuring phase synchrony in brain signals. *Hum. Brain Mapp.*, 8(4):194–208, 1999.
- [35] T. O. Laumann, A. Z. Snyder, A. Mitra, E. M. Gordon, C. Gratton, B. Adeyemo, A. W. Gilmore, S. M. Nelson, J. J. Berg, D. J. Greene, J. E. McCarthy, E. Tagliazucchi, H. Laufs, B. L. Schlaggar, N. U. F. Dosenbach, and S. E. Petersen. On the stability of BOLD fMRI correlations. *Cereb. Cortex*, 27(10):4719–4732, Oct. 2017.
- [36] S. H. Lee, The Schizophrenia Psychiatric Genome-Wide Association Study Consortium (PGC-SCZ), T. R. DeCandia, S. Ripke, J. Yang, P. F. Sullivan, M. E. Goddard, M. C. Keller, P. M. Visscher, N. R. Wray, The International Schizophrenia Consortium (ISC), and The Molecular Genetics of Schizophrenia Collaboration (MGS). Estimating the proportion of variation in susceptibility to schizophrenia captured by common SNPs. *Nat. Genet.*, 44(3):247–250, Mar. 2012.
- [37] J. Liu, J. Ji, G. Xun, L. Yao, M. Huai, and A. Zhang. EC-GAN: Inferring brain effective connectivity via generative adversarial networks. *Proc. Conf. AAAI Artif. Intell.*, 34(04):4852–4859, Apr. 2020.
- [38] Z. Liu, H. Mao, C.-Y. Wu, C. Feichtenhofer, T. Darrell, and S. Xie. A convnet for the 2020s, 2022.
- [39] L. Lyon. Dead salmon and voodoo correlations: should we be sceptical about functional MRI? *Brain*, 140(8):e53, Aug. 2017.
- [40] M. J. Maenner, Z. Warren, A. R. Williams, E. Amoakohene, A. V. Bakian, D. A. Bilder, M. S. Durkin, R. T. Fitzgerald, S. M. Furnier, M. M. Hughes, C. M. Ladd-Acosta, D. McArthur, E. T. Pas, A. Salinas, A. Vehorn, S. Williams, A. Esler, A. Grzybowski, J. Hall-Lande, R. H. N. Nguyen, K. Pierce, W. Zahorodny, A. Hudson, L. Hallas, K. C. Mancilla, M. Patrick, J. Shenouda, K. Sidwell, M. DiRienzo, J. Gutierrez, M. H. Spivey, M. Lopez, S. Pettygrove, Y. D. Schwenk, A. Washington, and K. A. Shaw. Prevalence and characteristics of autism spectrum disorder among children aged 8 years - autism and developmental disabilities monitoring network, 11 sites, united states, 2020. *MMWR Surveill. Summ.*, 72(2):1–14, Mar. 2023.

- [41] L. McInnes, J. Healy, N. Saul, and L. Großberger. Umap: Uniform manifold approximation and projection. *Journal of Open Source Software*, 3(29):861, 2018. doi: 10.21105/joss.00861. URL <https://doi.org/10.21105/joss.00861>.
- [42] P. R. Millar et al. Predicting brain age from functional connectivity in symptomatic and preclinical alzheimer disease. *Neuroimage*, 256(119228):119228, Aug. 2022.
- [43] E. Mishor, D. Amir, T. Weiss, D. Honigstein, A. Weissbrod, E. Livne, L. Gorodisky, S. Karagach, A. Ravia, K. Snitz, D. Karawani, R. Zirler, R. Weissgross, T. Soroka, Y. Endevelt-Shapira, S. Agron, L. Rozenkrantz, N. Reshef, E. Furman-Haran, H. Breer, J. Strotmann, T. Uebi, M. Ozaki, and N. Sobel. Sniffing the human body volatile hexadecanal blocks aggression in men but triggers aggression in women. *Sci. Adv.*, 7(47):eabg1530, Nov. 2021.
- [44] M. M. Monti. Statistical analysis of fMRI time-series: A critical review of the GLM approach. *Front. Hum. Neurosci.*, 5:28, Mar. 2011.
- [45] K. P. Murphy. *Probabilistic Machine Learning: An introduction*. MIT Press, 2022. URL [probml.ai](http://probml.ai).
- [46] A. Orlichenko, G. Qu, and Y.-P. Wang. Phenotype guided interpretable graph convolutional network analysis of fMRI data reveals changing brain connectivity during adolescence. In B. S. Gimi and A. Krol, editors, *Medical Imaging 2022: Biomedical Applications in Molecular, Structural, and Functional Imaging*, volume 12036, pages 294 – 303. International Society for Optics and Photonics, SPIE, 2022. doi: 10.1117/12.2613172. URL <https://doi.org/10.1117/12.2613172>.
- [47] A. Orlichenko, G. Qu, G. Zhang, B. Patel, T. W. Wilson, J. M. Stephen, V. D. Calhoun, and Y.-P. Wang. Latent similarity identifies important functional connections for phenotype prediction. *IEEE Transactions on Biomedical Engineering*, pages 1–12, 2022. doi: 10.1109/TBME.2022.3232964.
- [48] A. Orlichenko, G. Daly, J. W. Freeman, and Y.-P. Wang. ImageNomer: developing an interactive graphical analysis tool for examining fMRI and omics data. In B. S. Gimi and A. Krol, editors, *Medical Imaging 2023: Biomedical Applications in Molecular, Structural, and Functional Imaging*, volume 12468, page 1246812. International Society for Optics and Photonics, SPIE, 2023. doi: 10.1117/12.2654311. URL <https://doi.org/10.1117/12.2654311>.
- [49] A. Orlichenko, G. Daly, A. Liu, H. Shen, H.-W. Deng, and Y.-P. Wang. Imagenomer: developing an fmri and omics visualization tool to detect racial bias in functional connectivity, 2023.

- [50] A. Orlichenko, G. Qu, Z. Zhou, Z. Ding, and Y.-P. Wang. Angle basis: a generative model and decomposition for functional connectivity, 2023.
- [51] F. Parente and A. Colosimo. Modelling a multiplex brain network by local transfer entropy. *Sci. Rep.*, 11(1):15525, July 2021.
- [52] H.-J. Park, K. J. Friston, C. Pae, B. Park, and A. Razi. Dynamic effective connectivity in resting state fMRI. *Neuroimage*, 180(Pt B):594–608, Oct. 2018.
- [53] U. Pervaiz, D. Vidaurre, M. W. Woolrich, and S. M. Smith. Optimising network modelling methods for fMRI. *Neuroimage*, 211(116604):116604, May 2020.
- [54] J. D. Power, A. L. Cohen, S. M. Nelson, G. S. Wig, K. A. Barnes, J. A. Church, A. C. Vogel, T. O. Laumann, F. M. Miezin, B. L. Schlaggar, and S. E. Petersen. Functional network organization of the human brain. *Neuron*, 72:665–678, 2011.
- [55] S. Purcell, B. Neale, K. Todd-Brown, L. Thomas, M. A. R. Ferreira, D. Bender, J. Maller, P. Sklar, P. I. W. de Bakker, M. J. Daly, and P. C. Sham. PLINK: a tool set for whole-genome association and population-based linkage analyses. *Am. J. Hum. Genet.*, 81(3):559–575, Sept. 2007.
- [56] G. Qu et al. Ensemble manifold regularized multi-modal graph convolutional network for cognitive ability prediction. *IEEE Transactions on Biomedical Engineering*, 68(12):3564–3573, 2021. doi: 10.1109/TBME.2021.3077875.
- [57] A. Radford, J. W. Kim, C. Hallacy, A. Ramesh, G. Goh, S. Agarwal, G. Sastry, A. Askell, P. Mishkin, J. Clark, G. Krueger, and I. Sutskever. Learning transferable visual models from natural language supervision. *CoRR*, abs/2103.00020, 2021. URL <https://arxiv.org/abs/2103.00020>.
- [58] B. Rashid, M. R. Arbabshirani, E. Damaraju, M. S. Cetin, R. Miller, G. D. Pearlson, and V. D. Calhoun. Classification of schizophrenia and bipolar patients using static and dynamic resting-state fMRI brain connectivity. *Neuroimage*, 134:645–657, July 2016.
- [59] A. T. Reid, D. B. Headley, R. D. Mill, R. Sanchez-Romero, L. Q. Uddin, D. Marinazzo, D. J. Lurie, P. A. Valdés-Sosa, S. J. Hanson, B. B. Biswal, V. Calhoun, R. A. Poldrack, and M. W. Cole. Advancing functional connectivity research from association to causation. *Nat. Neurosci.*, 22(11):1751–1760, Nov. 2019.
- [60] C. Roehrig. Mental disorders top the list of the most costly conditions in the united states: \$201 billion. *Health Aff. (Millwood)*, 35(6):1130–1135, June 2016.

- [61] S. Sadeghi, D. Mier, M. F. Gerchen, S. N. L. Schmidt, and J. Hass. Dynamic causal modeling for fMRI with Wilson-Cowan-based neuronal equations. *Front. Neurosci.*, 14:593867, Nov. 2020.
- [62] H. Salehinejad, J. Kitamura, N. G. Ditkofsky, A. W. Lin, A. Bharatha, S. Suthiphoswan, H.-M. Lin, J. R. Wilson, M. Mamdani, and E. Colak. A real-world demonstration of machine learning generalizability in the detection of intracranial hemorrhage on head computerized tomography. *Scientific Reports*, 11, 2021.
- [63] S. Saponaro, A. Giuliano, R. Bellotti, A. Lombardi, S. Tangaro, P. Oliva, S. Calderoni, and A. Retico. Multi-site harmonization of MRI data uncovers machine-learning discrimination capability in barely separable populations: An example from the ABIDE dataset. *NeuroImage Clin.*, 35 (103082):103082, June 2022.
- [64] P. Sayegh, A. Arentoft, N. S. Thaler, A. C. Dean, and A. D. Thames. Quality of education predicts performance on the wide range achievement test-4th edition word reading subtest. *Archives of clinical neuropsychology : the official journal of the National Academy of Neuropsychologists*, 29 8: 731–6, 2014.
- [65] S. Schneider, J. H. Lee, and M. W. Mathis. Learnable latent embeddings for joint behavioural and neural analysis. *Nature*, 617(7960):360–368, May 2023.
- [66] X. Song, R. Li, K. Wang, Y. Bai, Y. Xiao, and Y.-P. Wang. Joint sparse collaborative regression on imaging genetics study of schizophrenia. *IEEE/ACM Trans. Comput. Biol. Bioinform.*, 20(2):1137–1146, Mar. 2023.
- [67] C. Sudlow, J. Gallacher, N. Allen, V. Beral, P. Burton, J. Danesh, P. Downey, P. Elliott, J. Green, M. Landray, B. Liu, P. Matthews, G. Ong, J. Pell, A. Silman, A. Young, T. Sprosen, T. Peakman, and R. Collins. UK biobank: An open access resource for identifying the causes of a wide range of complex diseases of middle and old age. *PLoS Med.*, 12(3):e1001779, Mar. 2015.
- [68] D. Szucs and J. P. Ioannidis. Sample size evolution in neuroimaging research: An evaluation of highly-cited studies (1990–2012) and of latest practices (2017–2018) in high-impact journals. *NeuroImage*, 221:117164, 2020. ISSN 1053-8119. doi: <https://doi.org/10.1016/j.neuroimage.2020.117164>. URL <https://www.sciencedirect.com/science/article/pii/S1053811920306509>.
- [69] D. Szucs and J. P. Ioannidis. Sample size evolution in neuroimaging research: An evaluation of highly-cited studies (1990-2012) and of latest practices (2017-2018) in high-impact journals. *Neuroimage*, 221(117164): 117164, Nov. 2020.

- [70] A. Taleb, M. Kirchler, R. Monti, and C. Lippert. Contig: Self-supervised multimodal contrastive learning for medical imaging with genetics. In *Proceedings of the IEEE/CVF Conference on Computer Vision and Pattern Recognition (CVPR)*, pages 20908–20921, June 2022.
- [71] Y.-F. Tan, C.-M. Ting, F. Noman, R. C.-W. Phan, and H. Ombao. Graph-regularized manifold-aware conditional wasserstein GAN for brain functional connectivity generation. 2022.
- [72] B. O. Turner, E. J. Paul, M. B. Miller, and A. K. Barbey. Small sample sizes reduce the replicability of task-based fMRI studies. *Commun. Biol.*, 1(1):62, June 2018.
- [73] L. van der Maaten and G. Hinton. Visualizing data using t-sne. *Journal of Machine Learning Research*, 9(86):2579–2605, 2008. URL <http://jmlr.org/papers/v9/vandermaaten08a.html>.
- [74] A. Vaswani, N. M. Shazeer, N. Parmar, J. Uszkoreit, L. Jones, A. N. Gomez, L. Kaiser, and I. Polosukhin. Attention is all you need. In *NIPS*, 2017.
- [75] Y. Wang, J. Lin, Q. Cai, Y. Pan, T. Yao, H. Chao, and T. Mei. A low rank promoting prior for unsupervised contrastive learning. *IEEE Transactions on Pattern Analysis and Machine Intelligence*, 45(3):2667–2681, 2023. doi: 10.1109/TPAMI.2022.3180995.
- [76] H. J. M. Warren, G. Ioachim, J. M. Powers, and P. W. Stroman. How fMRI analysis using structural equation modeling techniques can improve our understanding of pain processing in fibromyalgia. *J. Pain Res.*, 14: 381–398, Feb. 2021.
- [77] J. Zbontar, L. Jing, I. Misra, Y. LeCun, and S. Deny. Barlow twins: Self-supervised learning via redundancy reduction. 2021.
- [78] G. Zhang, B. Cai, A. Zhang, J. M. Stephen, T. W. Wilson, V. D. Calhoun, and Y.-P. Wang. Estimating dynamic functional brain connectivity with a sparse hidden markov model. *IEEE Trans. Med. Imaging*, 39(2):488–498, Feb. 2020.
- [79] G. Zhang, B. Cai, A. Zhang, Z. Tu, L. Xiao, J. M. Stephen, T. W. Wilson, V. D. Calhoun, and Y.-P. Wang. Detecting abnormal connectivity in schizophrenia via a joint directed acyclic graph estimation model. *Neuroimage*, 260(119451):119451, Oct. 2022.
- [80] C. Zhao, A. Liu, X. Zhang, X. Cao, Z. Ding, Q. Sha, H. Shen, H.-W. Deng, and W. Zhou. Clcls: Cross-omics linked embedding with contrastive learning and self attention for multi-omics integration with incomplete multi-omics data, 2023.

- [81] J. Zhao, J. Huang, D. Zhi, W. Yan, X. Ma, X. Yang, X. Li, Q. Ke, T. Jiang, V. D. Calhoun, and J. Sui. Functional network connectivity (FNC)-based generative adversarial network (GAN) and its applications in classification of mental disorders. *J. Neurosci. Methods*, 341(108756):108756, July 2020.
- [82] S. İcer, İrem Acer, and A. Baş. Gender-based functional connectivity differences in brain networks in childhood. *Computer Methods and Programs in Biomedicine*, 192:105444, 2020. ISSN 0169-2607. doi: <https://doi.org/10.1016/j.cmpb.2020.105444>. URL <https://www.sciencedirect.com/science/article/pii/S0169260719310685>.

## A Dynamic Dictionary Entries are Rank-1 Functional Connectivity Networks Associated with Maturation

One of the early goals of our research was to extend FC by treating it as a dynamic quantity, tapping into the dynamic nature of brain states. As an example approach, the Hidden Markov Model (HMM) has been widely used in neuroscience research [9]. This models the brain as being in discrete states with each time point containing a probability of transition to another state. Our group has performed a preliminary study using a sparse HMM (sHMM) to estimate dynamic FC [78]. This model directly fits the time-dependent BOLD data based on a Gaussian distribution with learned mean  $\mu_k$  and covariance matrix  $\Sigma_k$  at state  $k$ :

$$p(x_n^{(r)} | z_n^{(r)}_k = 1) = \frac{1}{(2\pi)^{d/2} |\Sigma_k|^{1/2}} \cdot \exp\left(-\frac{1}{2}(x_n^{(r)} - \mu_k)^\top \Sigma_k^{-1} (x_n^{(r)} - \mu_k)\right) \quad (9)$$

The Markov property gives the transition probability, which, when combined with the above model, gives the probability density that is fit to the data. An alternate approach is to use the Time-Varying Graphical Lasso (TVGL) model [24], also explored by our group [7].

We have conducted a preliminary study combining the TVGL model with dictionary learning using a database of learned rank-1 dictionary entries, with the belief that the rank-1 entries provide the simplest description of network-level activity on the scale of the whole brain. The problem is formulated as estimating the instantaneous rank-1 FC of a subject at each time point:

$$\mathbf{S}^{(t)} = \mathbf{X}_{:,t} \mathbf{X}_{:,t}^\top, \quad (10)$$

where  $\mathbf{X} \in \mathbb{R}^{N_d \times N_t}$  is a data matrix of  $N_d$  ROIs by  $N_t$  time points, and  $\mathbf{S}^{(t)}$  is the true instantaneous FC at time  $t$ . A dictionary is constructed as:

$$\begin{aligned} \mathcal{D} &= \{\mathbf{a}\mathbf{a}^\top \mid \mathbf{a} \in \mathbb{R}^{N_d \times 1}\}, \\ \hat{\mathbf{S}}^{(s,t)} &= \sum_{i=0}^{N_c} w_i^{(s,t)} \mathcal{D}_i, \end{aligned} \quad (11)$$

where  $\mathcal{D}$  is the FC dictionary,  $N_c = |\mathcal{D}|$  is the number of dictionary components,  $\mathcal{D}_i = \mathbf{a}\mathbf{a}^\top$  is the  $i^{\text{th}}$  rank-1 connectivity component,  $w_i^{(s,t)}$  is a learned weight, and  $\hat{\mathbf{S}}^{(s,t)}$  is the estimated FC for subject  $s$  at time  $t$ .

We perform training on a subset of subjects. Reconstruction loss is minimized along with a smoothness-promoting regularizer  $\alpha$  inspired by [7]. Weights

**Phenotype Signal in Dynamic Dict**

Phenotype	Min Entry Corr	Max Entry Corr	Scanner Task
Age	-0.263	+0.357	nback
Sex	-0.206	+0.163	emoid
Race	-0.246	+0.198	emoid
Intelligence	-0.151	+0.159	nback

Table 3: Minimum/maximum correlation of dictionary components with phenotype - higher absolute values indicate stronger signal.

are constrained to be non-negative.

$$\min_{\mathcal{D}, w_i^{(s,t)}} \left( \sum_{s,t} \|\mathbf{S}^{(s,t)} - \hat{\mathbf{S}}^{(s,t)}\|_F^2 + \alpha \sum_{s,t} \|\hat{\mathbf{S}}^{(s,t)} - \hat{\mathbf{S}}^{(s,t-1)}\|_F^2 \right) \quad \text{s.t. } w_i^{(s,t)} \geq 0, \quad (12)$$

We find the dictionary entries reveal qualitative changes in functional connectivity networks between children and young adults. Specifically, Figure 23 shows that children exhibit a diffuse connectivity whereas young adults have FCs which are organized into modules. Children also have higher average connectivity than young adults. We find a similar result for females vs males, where dictionary entries associated with females look like young adults, and dictionary entries associated with males look more like young children. The fact that our female dictionary components have high within-DMN connectivity is supported by other studies [19]. Additionally, as expected from our work in Section 3.2, we find highest correlation with our dictionary components is for age, lesser correlation for sex and race, and the smallest correlation for intelligence (see Table 3).

Additionally, we find that our dynamic dictionary is capable of better predictive performance compared to PCA or kSVD, although as shown in Figure 24, it is always inferior to a model simply using FC.

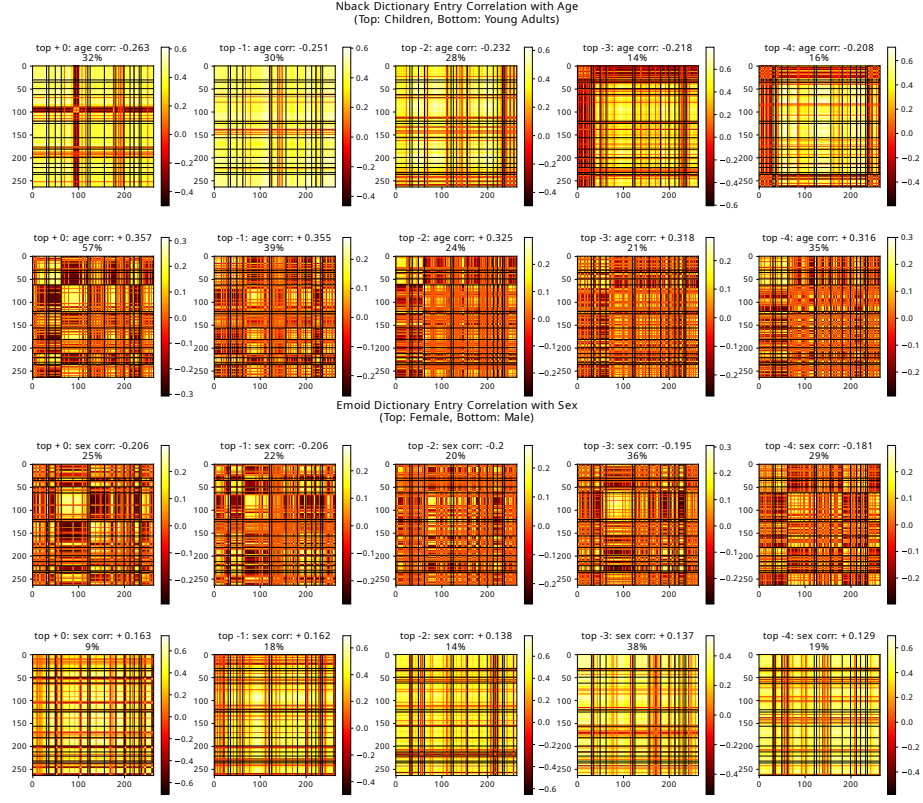


Figure 23: Top: Correlation of working memory task dictionary components with age. Young children have diffuse FC (top), while older children have FC that is much more modularized (bottom). Regions are listed in Table 1. Bottom: Correlation of emotion identification task dictionary components with sex. The dynamic dictionary decomposition is available at <https://github.com/aorliche/DynamicDict>.

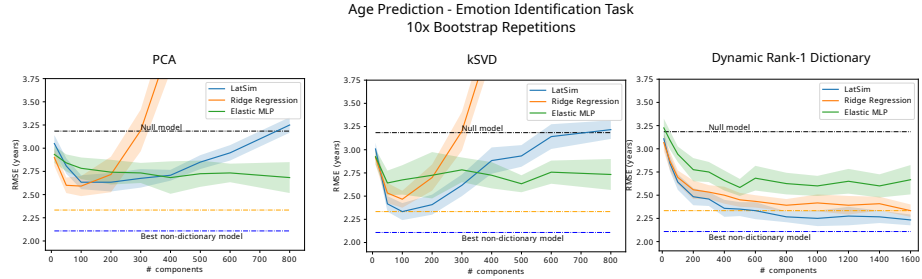


Figure 24: Comparison of age prediction error after dimensionality reduction by PCA, kSVD, and our dynamic rank-1 dictionary. Prediction was carried out using ridge regression, elastic MLP, and our Latent Similarity model.